NJC

Cite this: *New J. Chem.*, 2011, **35**, 1270–1279

www.rsc.org/njc

PAPER

Synthesis, structure, magnetism and theoretical study of a series of complexes with a decanuclear core $[Ln(III)_2Cu(II)_8]$ (Ln = Y, Gd, Tb, Dy)†‡

Ana Borta,[a] Erwann Jeanneau,[a] Yuri Chumakov,[a] Dominique Luneau,*[a] Liviu Ungur,[bc] Liviu F. Chibotaru*[b] and Wolfgang Wernsdorfer[d]

Received (in Montpellier, France) 25th November 2010, Accepted 28th April 2011
DOI: 10.1039/c0nj00931h

A family of four isomorph complexes with a decanuclear $[Cu_8Ln_2]$ core of general formula $[Ln_2Cu_8(\mu\text{-PyO})_{12}(\mu_4\text{-O})_2(\mu\text{-Cl})_2Cl_4(H_2O)_2]\cdot nH_2O$ [Ln(III) = Y(III) (**1**), Gd(III) (**2**), Tb(III) (**3**), Dy(III) (**4**); 2-PyOH = 2-hydroxypyridine] was isolated and structurally characterized. All compounds are isomorphs and may be viewed as a hexanuclear central core sandwiched in between two lateral dinuclear copper units. The temperature dependence of the magnetic susceptibility and the field dependence of the magnetization were investigated on polycrystalline samples. The yttrium compound **1** showed an overall behavior dominated by an antiferromagnetic interaction between the copper ions, while for compounds **2–4** the magnetic behavior indicated the addition of a ferromagnetic interaction with the lanthanide ions. The magnetic properties were computationally studied by means of fragment *ab initio* calculations. The calculation on the yttrium complex allowed determining the strength and sign of the Cu···Cu magnetic interactions considering three antiferromagnetic coupling constants: two within the central ($J_3 = -44$ cm^{-1}) and the lateral ($J_4 = -40$ cm^{-1}) copper dinuclear unit, and one ($J_5 = -24$ cm^{-1}) between the lateral and the central copper. Simulation of the magnetic behavior of the Dy (**4**) compound gave $J_1 = +0.25$ cm^{-1} for Dy–Dy and $J_2 = +2.0$ cm^{-1} for Dy–Cu pairs. The calculated *g* tensors of the copper(II) ions were found to be quite anisotropic and contributed *via* anisotropic exchange interactions, together with zero-field (crystal field) splitting on Ln, to the weak single-molecule magnet (SMM) behavior of **2**, **3** and **4**. Among them, the highest coercivity was found in the gadolinium complex (**2**), despite the fact that it is much less anisotropic than the other two. We explain this surprising result by a higher multiplicity of the ground spin term in **2** compared to the ground manifolds of states in **3** and **4**. Besides, due to relatively large Cu–Gd interaction, the ground exchange term in **2** has enough separation from excited exchange terms, which makes the barrier of reversal of magnetization efficient in this complex.

[a] *Université Claude Bernard Lyon 1, Laboratoire des Multimatériaux et Interfaces (UMR 5615), Campus de La Doua, 69622 Villeurbanne Cedex, France. E-mail: luneau@univ-lyon1.fr*
[b] *Afdeling Kwantumchemie en Fysicochemie, Katholieke Universiteit Leuven, Celestijnenlaan 200F, B-3001 Leuven, Belgium. E-mail: Liviu.Chibotaru@chem.kuleuven.be*
[c] *INPAC-Institute of Nanoscale Physics and Chemistry, Katholieke Universiteit Leuven, Celestijnenlaan 200F, B-3001, Leuven, Belgium*
[d] *Institut Néel-CNRS, BP166, 25 Avenue des Martyrs, 38042 Grenoble Cedex 9, France*

† This article is part of a themed issue on Molecular Materials: from Molecules to Materials, commissioned from the MolMat2010 conference.

‡ Electronic supplementary information (ESI) available: Figures of the crystal packing and TGA diagrams. CCDC reference numbers 803518–803521. For ESI and crystallographic data in CIF or other electronic format see DOI: 10.1039/c0nj00931h

Introduction

Investigations for polynuclear metal complexes exhibiting Single Molecule Magnet (SMM) behavior is one of the most appealing and challenging questions in the field of magnetic materials.[1,2] To be an SMM, a complex must have a high-spin ground state (S) with a strong uniaxial magnetic anisotropy ($D < 0$) to induce two orientations of the magnetization that are well-separated in energy.[2,3] The way the magnetization is retained in one direction depends on the energy barrier, roughly given by $|D|S^2$.[4] Thus, the larger D and S, the higher the barrier and the longer the magnetization should be retained.

Most preliminary efforts devoted to SMMs have concentrated on the synthesis of large clusters with high-spin ground

states (S).[5–10] In this way, the field has greatly benefited from previous research in molecular magnetism, which has lead to well established correlations between magnetic interactions and structure.[11] Frustratingly, the blocking temperatures remained low. From these results, it became obvious that increasing only the spin makes no sense, as long we do not know how to built polynuclear systems with strong molecular anisotropy. Thus, the main focus of the current investigation is to design systems with a large molecular anisotropy as well to understand the relationships between structure and anisotropy.[12,13] From this point of view, lanthanide ions attract attention since some of them are associated with large spin values and strong Ising-type magnetic anisotropy due to spin–orbit coupling.[14] This was demonstrated by the discovery that some lanthanide-phthalocyanine mononuclear complexes exhibit SMM behavior. [15,16] However, most SMMs incorporating lanthanides concern systems in which they are associated with 3d transition metal ions. [17,18] Indeed, in such systems, two cumulative effects are expected. First, the lanthanide ions should increased the overall anisotropy. Second, the interplay of the magnetic exchange interaction between d and f ions, even if they are usually rather small, is expected to increase the ground spin state. For instance, Gd···Cu, Dy···Cu and Tb···Cu interactions are known to be generally ferromagnetic.[19–22]

Along the lines of this strategy, we previously synthesized Ln–Cu architectures with controlled nuclearities, with the challenging goal of scaling-up the ground spin state as well as the anisotropy.[17,23] In the present paper, we report the syntheses, crystal structure and magnetic studies of $[Ln_2Cu_8]$-type decanuclear complexes [Ln = Y (**1**), Gd (**2**), Tb (**3**) and Dy (**4**)]. The synthesis of such compounds was first described for yttrium in 1991 by S. Wang *et al.*[24] Given the arrangement of the Cu(II) and Ln(III) ions in this compound, we thought that the synthesis of analogues with lanthanides ions having strong magnetic anisotropy [Dy(III), Tb(III)] could result in molecular systems with high spin and strong anisotropy presenting SMM behavior.

Experimental section

All chemicals and solvents were purchased from commercial suppliers and used as received. All preparations and manipulations were performed under aerobic conditions.

Syntheses of $[Y_2Cu_8]$ and $[Ln_2Cu_8]$ complexes

All compounds were obtained following the same procedure. Hydroxypyridine (2-PyOH) was dissolved (0.114 g; 1.2 mmol) in methanol (10 mL), and a solution of 0.2 mmol of metal chloride salt in 5 mL of methanol was added dropwise ($YCl_3{\cdot}6H_2O$, 0.073 g, 0.2 mmol, M = 365 g mol^{-1}; $GdCl_3{\cdot}6H_2O$, 74.34 g, 0.2 mmol, M = 371.7 g mol^{-1}; $DyCl_3{\cdot}6H_2O$ 0.075 g, 0.2 mmol, M = 376.95 g mol^{-1}; $TbCl_3{\cdot}6H_2O$ 0.0746 g, 0.2 mmol, M = 373.37 g mol^{-1}). The resulting light yellow solution was stirred for 10 min. Following this, a solution of 0.8 mmol of $CuCl_2{\cdot}2H_2O$ (85 mg; M = 170.48 g mol^{-1}) in 5 mL of methanol was added. To the resulting light green solution was added triethylamine dropwise, leading to a deep green solution and until the appearance of a light green precipitate (~0.21 mL). The solution was then filtered to remove the precipitate and left to slow evaporate at room temperature. After 3 d, green crystals of $[Ln_2Cu_8]$ [Ln = Y(**1**) , Gd (**2**) , Tb (**3**), Dy (**4**)] suitable for single-crystal X-ray diffraction analyses were obtained in 60–70% yield. They were isolated by filtration and washed with a small amount of methanol. The analytical purity of each compound was checked by elemental analysis: Anal. calc. for **1** $Cu_8Y_2C_{60}H_{92}N_{12}O_{36}Cl_6$ (containing $22H_2O$): C, 29.34; H, 3.78; Cl, 8.66; Cu, 20.70; Y, 7.24; N, 6.84. Found C, 29.1; H, 3.6; Cl, 8.54; Cu, 20.63; Y, 7.20; N, 6.75%. Calc. for **2** $Cu_8Gd_2C_{60}H_{98}N_{12}O_{39}Cl_6$ (containing $25H_2O$): C, 27.21; H, 3.70; Cl, 8.05; Cu, 19.21; Gd, 11.87; N, 6.35. Found C, 27.18; H, 3.47; Cl, 7.84; Cu, 19.13; Gd, 11.69; N, 6.24%. Calc. for **3** $Cu_8Dy_2C_{60}H_{94}N_{12}O_{37}Cl_6$ (containing $23H_2O$): C, 27.48; H, 3.59; Cl, 8.13; Cu, 19.40; Dy, 12.39; N, 6.41. Found. C, 27.57; H, 3.48, Cl; 7.03; Cu, 19.35; Dy, 12.26; N, 6.42%. Calc. for **4** $Cu_8Tb_2C_{60}H_{86}N_{12}O_{33}Cl_6$ (containing $19H_2O$): C, 23.29; H, 3.38; Cl, 8.38; Cu, 19.99; Tb, 12.50; N, 6.61. Found C, 23.13; H, 3.16; Cl, 8.26; Cu, 19.91; Tb, 12.43; N, 6.49%.

Crystallography

Suitable crystals were mounted on a Nonius Kappa CCD diffractometer using Mo-Kα radiation (λ = 0.71073 Å) and equipped with a CCD area detector. Intensities were collected at 150 K by means of the program COLLECT[25] with a step rotation angle of 1° for the θ angle. Reflection indexing, Lorentz polarization correction, peak integration and background determination were carried out with DENZO[26] frame scaling, and unit cell parameter refinements were made through the program SCALEPACK.[26] The structures were solved and refined on F^2 using CRYSTAL software.[27] All non-hydrogen atoms were refined with anisotropic thermal parameters. The hydrogen atoms were included in the final refinement model in calculated positions with isotropic thermal parameters.

Magnetic measurements

DC magnetic data were measured using a Quantum Design MPMS-XL5 SQUID magnetometer equipped with an EVER Cool system at the University Claude Bernard Lyon 1 on polycrystalline samples in the temperature range 2 to 300 K with an applied field of 0.1 T for magnetic susceptibility and at 2 K in the 0–5 T range for magnetization. To avoid orientation in the magnetic field, the gadolinium, terbium and dysprosium samples were pressed into a home-made Teflon sample holder equipped with a piston. The data were corrected for the diamagnetism of the constituent atoms using Pascal's constants.

Micro-SQUID

Magnetization measurements on single-crystals were performed at the Institut Néel in Grenoble with an array of micro-SQUIDs.[3] This magnetometer works in the temperature range ~0.04–7 K with applied fields up to 14 kOe. The time resolution is approximately 1 ms. The field can be applied in any direction of the micro-SQUID plane with a precision smaller than 0.1° by separately driving three orthogonal coils.

The field was then aligned with the easy axis of magnetization using a transverse field method.[3b]

Computational details

The complexes **1–4** were too large to be treated entirely by existing explicitly correlated *ab initio* methodologies. Therefore, they were computationally studied by means of fragment calculations. It is not a trivial task to build reliable fragments that will not change much the energy spectrum of a given metal site. In this problem, one has to rely mainly on chemical intuition alone. The treatment of the influence of neighboring metal ions is another difficult question. In this work, we have modeled neighboring copper ions by Zn^{2+}-AIMP developed by Lopez-Moraza *et al.*,[28] while the lanthanides were computationally treated as La^{3+}-AIMP developed by DeGraaf *et al.*[29]

All *ab initio* calculations were performed with the MOLCAS 7.6 program package.[30] By this approach, the relativistic effects are treated in two steps, both based on the Douglas-Kroll approximation.[31] Scalar relativistic effects are included in the basis set generation by employing ANO-RCC basis sets,[32] which were used for the determination of the complete active space self-consistent field (CASSCF) spin free energies and wave functions. Dynamical correlation is added by a complete active space second order perturbation theory (CASPT2). Standard IPEA (0.25) and imaginary shift (0.1) were used in order to exclude any possible intruder state problems. The spin–orbit coupling was treated by the restricted active space state interaction (RASSI),[33] which uses the spin-free eigenstates as input. The spin–orbit interaction was computed on the basis of all-computed spin-free states in the case of copper, while in the case of lanthanides, the maximum number of states allowed by the hardware were taken into account. The resulting spin–orbit energies and functions were used by the developed program SINGLE_ANISO,[34] which is presently a module in MOLCAS 7.6 to compute all magnetic properties and parameters of the pseudospin Hamiltonians for the computed fragment. The lowest spin-orbital states were further taken for the exchange coupling between metal sites and were treated within the Lines model,[35] which approximates the anisotropic exchange coupling by a single parameter for an interacting metal pair. The Lines parameters are, thus, the only fitting parameters of the theory. On the basis of exchange eigenstates, the magnetic properties of the polynuclear complex and parameters of pseudospin Hamiltonians are calculated. The Lines exchange coupling and subsequent computation of the magnetic properties of the polynuclear cluster was done by the program POLY-ANISO.[34]

Results and discussion

Syntheses

The first hetero-metal complexes with lanthanides and 2-hydroxypyridine (2-PyOH) as the ligand had a metal core of formula $[Cu_4Ln_2]$ (Ln = Gd and Dy) and were published in 1989 by R. E. P. Winpenny *et al.*[36] These complexes were obtained by mixing the ligand with copper hydroxide and lanthanide nitrate in methanol. Following on, other Ln/Cu ratios were obtained, depending on the lanthanide ion, as often observed due to lanthanide contraction but also depending on the synthesis procedure. Thus, with lanthanum, the same method as above gave a complex of formula $[Cu_4La_4]$,[37] while starting from pre-formed copper pyridone complexes and reacting with lanthanide nitrate and 2-PyOH resulted in different complexes, such as $[La_8Cu_{12}]$,[38] $[Yb_2Cu_2]$[39] and $[La_2Cu_2]$ [La Cu_3].[40] In another route, Wang *et al.* used lanthanide nitrate and a mixture of copper methoxide and $CuCl_2$ instead of copper hydroxide, and gave in methanol the decanuclear complexes $[Y_2Cu_8]$[24] and $[Nd_2Cu_8]$.[41] These complexes have choro-bridged copper(II) and nitrate ions coordinated to Yttrium in $[Y_2Cu_8]$,[24] and none in the neodymium compound $[Nd_2Cu_8]$.[41]

Owing to the structural arrangement of the lanthanide and copper(II) ions in these decanuclear systems, we were interested to study their analogues with magnetic lanthanide ions, such as Gd(III), and moreover Tb(III) and Dy(III). First, we used the same method as described by Wang *et al.* for $[Nd_2Cu_8]$.[41] This afforded well chapped crystals, but which surprisingly did not diffract. Following this, we used a different synthesis procedure, in which we reacted PyOH in methanol with the chloride salts of Cu(II) and Ln(III), and some drops of Et_3N. This yielded well chapped dark green crystals of the $[Ln_2Cu_8]$ compound in 60–70% yield that were suitable for single-crystal X-ray diffraction analysis. Elemental analysis and single-crystal X-ray diffraction analysis established that these compounds have the formula: $[Ln(III)_2Cu(II)_8(\mu\text{-}PyO)_{12}(\mu_4\text{-}O)_2(\mu\text{-}Cl)_2Cl_4(H_2O)_2]\cdot nH_2O$ with Ln = Y (**1**), Gd (**2**), Tb (**3**) and Dy (**4**), and n = 22(**1**), 25(**2**), 19(**3**) and 23(**4**). The complexes reported here have a similar decanuclear core $\{Ln(III)_2Cu(II)_8(\mu\text{-}PyO)_{12}(\mu_4\text{-}O)_2(\mu\text{-}Cl)\}$ as that found for $[Cu_8Y_2]$[24] and $[Cu_8Nd_2]$,[41] but the overall molecular structure is different. In compounds **1–4** there are four more coordinated chloride ions: two are on each of the lanthanides ions and the last two are on the copper ions.

Crystal and molecular structures

All compounds **1–4** are isomorphs and have the same molecular structure, $[Ln_2Cu_8(\mu\text{-}PyO)_{12}(\mu_4\text{-}O)_2(\mu\text{-}Cl)_2Cl_4(H_2O)_2]$, crystallizing with water molecules in the $P2_1/c$ space group of the monoclinic system. Table 1 summarizes the crystallographic data and refinement details for compounds **1–4**.

The asymmetric unit consists of one molecule of the cluster localized in a general position plus a second molecule lying about an inversion center. In the following, the description refers to the molecule in the general position but holds also for the one on the inversion center. The $[Ln_2Cu_8(\mu\text{-}PyO)_{12}(\mu_4\text{-}O)_2(\mu\text{-}Cl)_2Cl_4(H_2O)_2]$ cluster (Fig. 1) can be seen as a hexanuclear central core formed by two lanthanide ions and two dinuclear copper moieties sandwiched in between two lateral dinuclear copper units. The twelve ligands are tri-coordinated. For six ligands, the oxygen atom is bridging an Ln(III) ion and a Cu(II) ion from the hexanuclear core, while the nitrogen is coordinated with one Cu(II) ion from lateral copper dinuclear units (Fig. 1). In the case of the last four ligands, the oxygen atom is bridging Cu(II) ions of the lateral dinuclear moieties while the nitrogen is coordinated to one Cu(II) ion of the hexanuclear central core (Fig. 2).

Table 1 Crystal data and structure refinement parameters for compounds **1–4**

Parameters	$[Y_2Cu_8]$ (**1**)	$[Gd_2Cu_8]$ (**2**)	$[Tb_2Cu_8]$ (**3**)	$[Dy_2Cu_8]$ (**4**)
Formula	$C_{60}H_{52}Cl_6Cu_8N_{12}O_{16}Y_2 \cdot (H_2O)_{13}$	$C_{60}H_{52}Cl_6Cu_8Gd_2N_{12}O_{16} \cdot (H_2O)_9$	$C_{60}H_{52}Cl_6Cu_8N_{12}O_{16}Tb_2 \cdot (H_2O)_9$	$C_{60}H_{52}Cl_6Cu_8Dy_2N_{12}O_{16} \cdot (H_2O)_9$
fw/g mol^{-1}	2096.06	2232.73	3357.15	3364.85
Crystal system	Monoclinic	Monoclinic	Monoclinic	Monoclinic
Space group	$P2_1/n$	$P2_1/n$	$P2_1/n$	$P2_1/n$
a/Å	16.5041(16)	16.4096(13)	16.717(3)	16.6165(13)
b/Å	19.2258(18)	19.7554(15)	19.241(4)	19.3662(15)
c/Å	45.343(4)	45.583(4)	45.634(9)	45.961(4)
α (°)	90	90	90	90
β (°)	96.870(2)	95.465(1)	96.53(3)	96.779(1)
γ (°)	90	90	90	90
V/Å^3	14284(2)	14710(2)	14583(5)	14686.8(2)
Z	6	6	4	4
T/K	293	293	293	293
$\lambda_{Mo\text{-}K\alpha}$/Å	1.71073	0.71073	0.71073	0.71073
D/g cm^{-3}	1.625	1.622	1.639	1.522
μ/mm^{-1}	3.18	3.31	3.37	3.42
$R(F_o)^a$	0.059	0.047	0.066	0.045
$R_w(F_o)^b$	0.222	0.144	0.182	0.148
S	1.04	1.17	0.103	1.17

^{a} $R(F) = \Sigma\,||F_o| - |F_c||/\Sigma|F_o|$. ^{b} $R_w(F) = \Sigma[w((F_o^2 - F_c^2)^2/\Sigma wF_o^4]^{1/2}$.

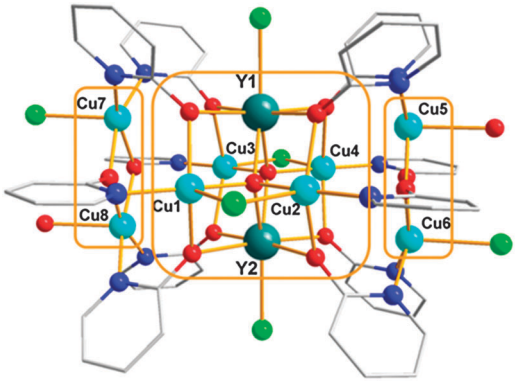

Fig. 1 Representation of the complex $[Y_2Cu_8(\mu\text{-PyO})_{12}(\mu_4\text{-O})_2(\mu\text{-Cl})_2Cl_4(H_2O)_2]$ (**1**).

In the central core there are two μ_4-O oxo groups (O1 and O2) (Fig. 2). Each of them is bridging two lanthanide ions and two copper ions. Each lanthanide ion is also bridged with the four copper ions *via* oxygen atoms of four 2-hydroxypyridine ligands. The lanthanide ions are heptacoordinated (Fig. 2) with a capped trigonal prism geometry, formed of six oxygen atoms (O1, O2, O3, O4, O5, O6) and capped by a chloride ion (Cl4). The Ln–O and Ln–Cl distances are normal and in good agreement with those found in the literature. The distance between the two lanthanide ions is close to 3.8 Å, and that between the lanthanide and the copper ions is close to 3.4 Å.

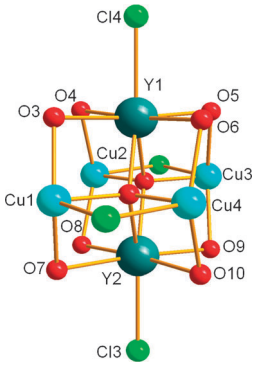

Fig. 2 Representation of the hexanuclear central core $\{Y_2Cu_4\}$.

The copper ions have a pentacoordinated environment and two geometries can be observed. For copper ions of the central core (Cu1–Cu2, Cu3–Cu4), the calculated Addison factors[42] (τ = 0.68 for **1**), taking into account the two largest angles O–Cu–O and N–Cu–O, are in agreement with distorted trigonal bipyramid geometries (τ = 1 for geometry ideal). This consists of an oxygen atom of the group μ_4-O, a bridging chloride ion and two atoms of oxygen and nitrogen ligands, which are in a plane (N4, O1, Cl1) (Fig. 3a). The copper ions belonging to the lateral dinuclear copper moieties (Cu5–Cu6, Cu7–Cu8) also have a pentacoordinated environment, but here the Addison factor[42] (τ = 0.04) indicates a square-based pyramid geometry (τ = 0 for geometry square-based pyramid) consisting of two nitrogen atoms and two oxygen atoms of the ligand, and a chloride ion or water molecule in the apical position (Fig. 3b).

Examination of the molecular packing in $[Ln_2Cu_8]$ compounds evidences narrow channels (Fig. 1S) along the two *a* and *b* axes, which look larger along the median axis.

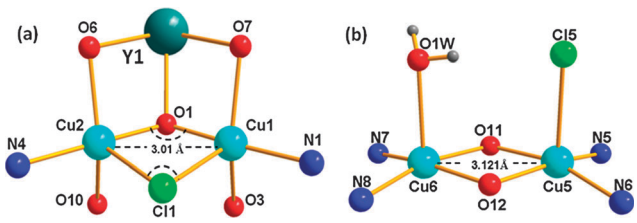

Fig. 3 Representation of the coordination environment around the copper ions within the dinuclear moiety of the hexanuclear central core $\{Y_2Cu_4\}$ (a) and within the lateral moieties (b).

These channels may explain the numerous water molecules of crystallization, and these diffraction peaks decay during data collection. The presence of the many water molecules was determined using the SQUEEZE program from Crystals.[27,43] After the atomic structure of the complex was completed, there still were large cavities where delocalized electron density was present. These remaining weak density peaks could thus not be attributed to localized water molecules. The discrete Fourier transform of the observed density in the water molecules' area was calculated and incorporated as the water molecules' contribution to the structure factors and refinement procedure through the SQUEEZE algorithm[44] in PLATON. This was confirmed by thermogravimetric analysis (TGA) carried out in the range 25–500 °C. For all samples, a mass loss of ~12% with an endothermic behavior was observed below ~200 °C (Fig. 2S) that we attributed to the departure of water molecules of crystallization. Around 250 °C, there were exothermic peaks that we attributed to the departure of coordinated water molecules. Above 270 °C, compounds gradually decomposed. From these TGA studies and depending on the compound, we calculated an average of 15 water molecules per $[Ln_2Cu_8]$ unit, in agreement with analysis and crystal structure data.

Magnetic properties

$[Y_2Cu_8]$ (1)

As the yttrium(III) ion is diamagnetic, the magnetic properties of complex $[Y_2Cu_8]$ were studied to determine the strength of the magnetic interaction between the Cu(II) ions within the series of compounds. The magnetic properties of compound **1** are reported in Fig. 4.

At 300 K, the χT product of 3.88 cm^3 K mol^{-1} is far above the expected value for eight magnetically independent Cu(II) ions (3.00 cm^3 K mol^{-1} for $g = 2$). Upon cooling, χT continuously decreases to 50 K and then rapidly reaches zero at 2 K, where an inflection point is observed. This feature indicates dominant antiferromagnetic interactions between the Cu(II) ions, which are strong since χT is far from saturation at 300 K. At the same time, Fig. 4 shows a low excitation energy to magnetic states ($S \neq 0$) in the complex, which is due to competing antiferromagnetic interactions (see below).

$[Gd_2Cu_8]$ (2)

The electronic configuration of the gadolinium(III) ion is $4f^7$. Thus, this lanthanide ion is isotropic and the magnetic moment is not influenced by the spin–orbit coupling. The magnetic properties of compound **2** are reported in Fig. 5. At 300 K, the χT value of 19.52 cm^3 K mol^{-1} is slightly larger than the expected value for two Gd(III) and eight Cu(II) (18.76 cm^3 K mol^{-1} for $g = 2$). Upon cooling, χT decreases slightly down to 200 K, then increases to reach a maximum at 30 K (20.31 cm^3 K mol^{-1}) and then decreases abruptly below this temperature. The decrease of χT above 200 K is ascribed to the prevalence of the Cu···Cu interactions, as found for the yttrium compound. The increase is the contribution of the Cu···Gd interactions, which tend to align ferromagnetically the spins of two Gd ions at low temperature. Such interactions were previously found to be ferromagnetic in related Cu_2Gd_2 and Cu_4Gd_2 compounds with 6-chloro-2-hydroxypyridine,[45] and antiferromagnetic in recently synthesized Cu_5Gd_4.[46] In **2**, the decreasing of χT at low temperature cannot be attributed solely to intermolecular interactions or to zero field splitting (ZFS) in the ground spin term (the maximum of χT lies at 30 K). Therefore, it can only originate from antiferromagnetic interactions of Gd_2 and Cu_8 subsystems, giving a total spin of the ground term smaller than $2 \times S_{Gd} = 14$.

A further study was conducted on a single-crystal using the technique micro-SQUID. At very low temperatures (0.04–1 K), we observed a hysteresis cycle (Fig. 6), which is the signature of slight anisotropy. However, as previously observed for other Cu···Gd systems, the origin of this small magnetic anisotropy is difficult to elucidate.

$[Tb_2Cu_8]$ (3)

The magnetic properties of compound **3** are reported in Fig. 7. At 300 K, χT has a value of 27.31 cm^3 K mol^{-1}, which is close to the expected value for eight Cu(II) and two magnetically-independent Tb(III) (27.6 cm^3 K mol^{-1}). Upon cooling, χT increases continuously up to 28 K, where it reaches a

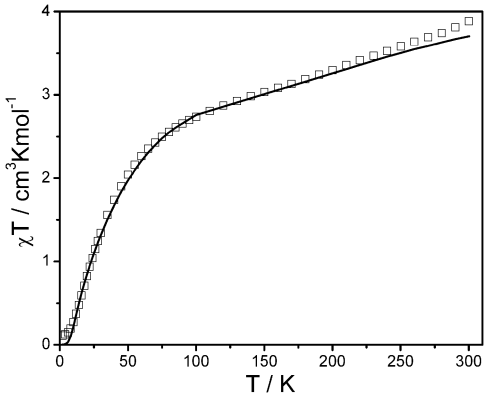

Fig. 4 Temperature dependence of the χT product for compound $[Y_2Cu_8]$ (**1**). The squares represent the experimental data and the solid line corresponds to the simulation based on *ab initio* calculations (see the text).

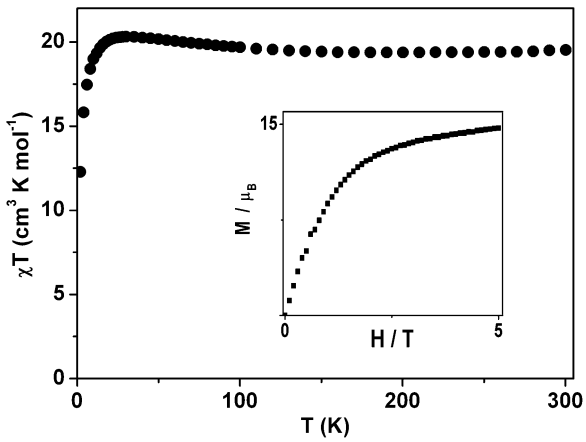

Fig. 5 Temperature dependence of the χT product and magnetization at 2 K (inset) for $[Gd_2Cu_8]$ (**2**).

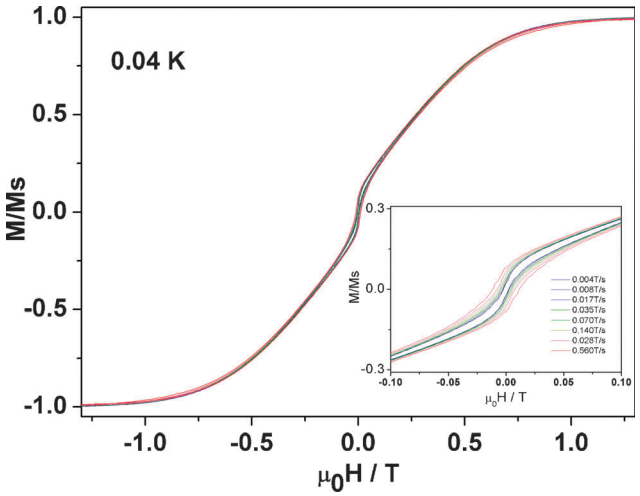

Fig. 6 Magnetization curves for single-crystals of $[Gd_2Cu_8]$ (**2**) at 0.04 K using various field sweep rates.

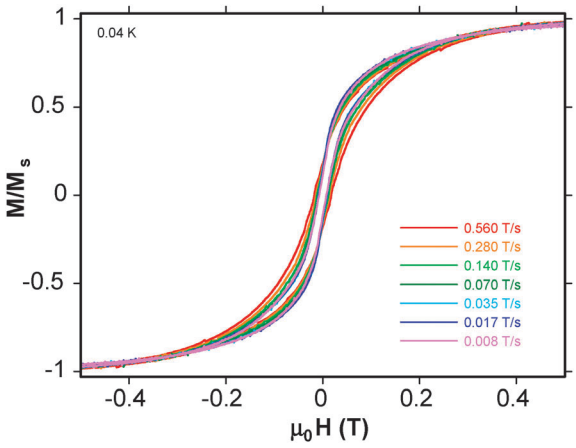

Fig. 8 Magnetization curves for single-crystals of $[Tb_2Cu_8]$ (**3**) at 0.04 K using various field sweep rates.

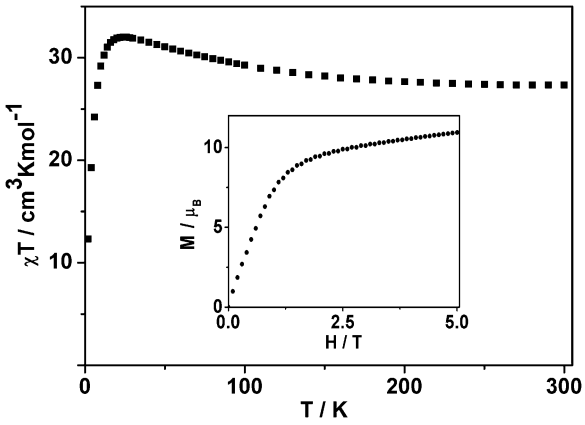

Fig. 7 Temperature dependence of the χT product and magnetization at 2 K (inset) for $[Tb_2Cu_8]$ (**3**).

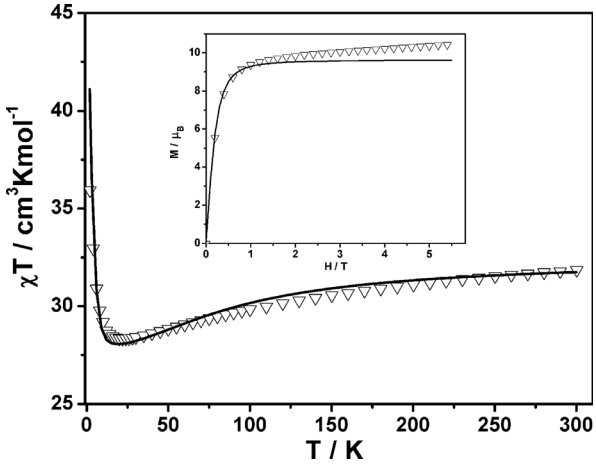

Fig. 9 Temperature dependence of the χT product and the magnetization at 2 K (inset) for $[Dy_2Cu_8]$ (**4**). The triangles are the experimental data and the solid lines are the simulations based on *ab initio* calculations (see the text).

maximum value of 31.99 cm^3 K mol^{-1} and then decreases down to 2 K, where it reaches a value of 12.3 cm^3 K mol^{-1}. This behavior is similar to the case of Gd_2Cu_8 (Fig. 5) and can be explained by the same reasons. The steeper decreasing of χT at low temperature is due to a stronger crystal field splitting on Tb compared to the ZFS on Gd. The magnetization *vs.* magnetic field at 2 K shows the characteristic behavior generally observed for systems with Tb(III). At very low temperatures, this compound shows hysteresis cycles of magnetization (Fig. 8).

$[Dy_2Cu_8]$ (4)

The magnetic properties of compound **4** are reported in Fig. 9. At 300 K, χT has a value of 31.63 cm^3 K mol^{-1}, which is in good agreement with eight Cu(II) and two magnetically-independent Dy(III) (31.3 cm^3 K mol^{-1}). Upon cooling, χT decreases continuously down to 20 K, reaches a minimum value of 28.33 cm^3 K mol^{-1}, and then increases rapidly and continuously, and at 2 K the χT value is 35.92 cm^3 K mol^{-1}. The preliminary decrease from room temperature is ascribed not only to the antiferromagnetic interaction between Cu···Cu, as in the gadolinium (**2**) compound, but also to the temperature depopulation of strongly split crystal field sublevels of Dy(III) (Table 4), while the sudden growth of χT below 20 K is the signature of ferromagnetic interactions in the Cu(II)–Dy(III) and Dy(III)–Dy(III) pairs.

The χ-SQUID measurements performed at very low temperatures show small hysteresis cycles (Fig. 10).

Ab initio calculation of the magnetic properties

In an effort to gain a better description of the origin of the magnetic properties of complexes **1–4**, we investigated the lowest spin states and spin–orbit multiplets by means of fragment *ab initio* calculations, as described in Experimental section. The magnetic properties of individual metal fragments were calculated fully *ab initio* using the program Single_aniso, and on their basis the magnetism of polynuclear compounds

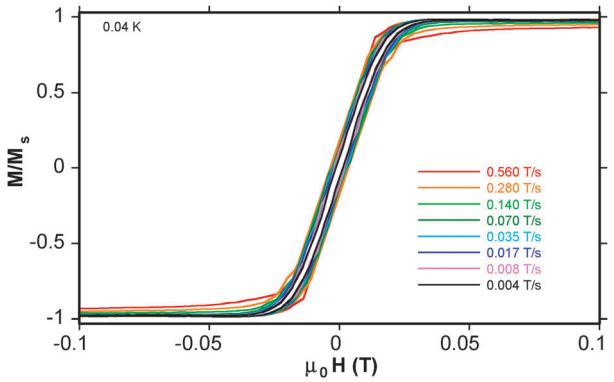

Fig. 10 Magnetization curves for single-crystals of $[Dy_2Cu_8]$ (**4**) at 0.04 K using various field sweep rates.

were simulated using the program Poly_aniso, as described previously.[12,47,48]

$[Y_2Cu_8]$ (1)

Since yttrium is diamagnetic, the magnetism of **1** comes only from the unpaired electrons of the copper ions. The structures of the calculated copper fragments for $[Y_2Cu_8]$ (**1**) are given in Fig. 11.

The results of *ab initio* calculations of all copper fragments are given in Table 2 for the low-lying Kramers doublets and in Table 3 for the g tensors in the lowest Kramers doublets.

In the Cu1 fragment, from central core (Fig. 11a), the nitrogen and the *trans*-oxygen from the first coordination sphere lie almost in line with the Cu. At the same time, the other two oxygens and the chlorine make angles of 107, 113 and 135°, which means that geometrically the first coordination sphere is close to trigonal bipyramidal (TBP). The *ab initio* calculations also show that the electronic properties are close to TBP. Indeed, Fig. 12a shows that the magnetic orbital of Cu, containing the unpaired electron, is predominantly of d_{z^2} type and is directed along the "trigonal axis" O–Cu–N (Fig. 11a). Moreover, $g_z < g_{x,y}$ for all four fragments Cu1–Cu4, which is also to be expected for TBP coordination. The deviation from C_3 symmetry of these fragments is reflected in the different values of g_x and g_y.

In the Cu5 fragment, from lateral moieties (Fig. 11b), the two oxygens and the two nitrogens from the first coordination sphere of the Cu lie practically in one plane, while the apical

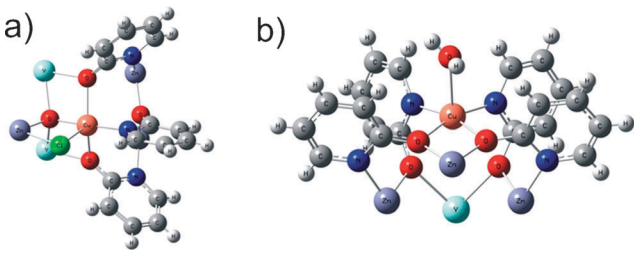

Fig. 11 Structures of the calculated Cu fragments: (a) Fragment Cu1, similar to fragments Cu2, Cu3 and Cu4. (b) Fragment Cu5, similar to fragment Cu8. Fragments Cu6 and Cu7 differ from Cu5 by substitution of the water ligand by a chlorine. Due to the isomorphism of complexes **1–4**, this copper fragment model was used for the whole series.

oxygen makes an angle of *ca.* 86° with this plane. Despite the fact that the geometry of this coordination is far from square pyramidal (SP), the magnetic orbital on Cu is almost of net $d_{x^2-y^2}$ character and $g_z > g_{x,y}$ (Table 3). Surprisingly, $g_x \approx g_y$ for all the centers of this type, Cu5–Cu8, which is to be generally expected for SP with a C_4 symmetry axis. A similar situation was encountered in low-symmetric $[Mo(III)(CN)_7]^{4-}$, where the degeneracy of the two main values of the g tensor was explained by closely spaced magnetic orbitals on Mo(III).[49] In the present case, however, the degeneracy of g_x and g_y seems to be rather accidental.

As can be seen from Table 2, the obtained excited states of the copper ions are quite low in energy, which is a sign of stronger than usual spin–orbit coupling effects for these copper ions. This is reflected in the large values of the g tensors for the ground Kramers doublets (Table 3) and the high χT at 300 K of individual Cu fragments as compared to pure $S = 1/2$ ($\approx$0.375 cm^3 K mol^{-1}). Actually, the values of $\Delta g_\alpha = g_\alpha - 2$ from Table 3 seem to be exaggerated. This is a known drawback of the CASSCF/MS-CASPT2 approach when it involves complete active space (CAS)-only molecular orbitals of the ligand-field type. Applied to strongly covalent transition metal complexes, it leads to the deviation of Δg_α from experimental values of *ca.* 50%.[49–51] The reason for this is the strong ionic character of the CASSCF wave functions, and improving this is achieved by adding frontier orbitals of predominantly ligand-type to the CAS. For instance, in the case of small copper complexes like $CuCl_4^{2-}$, the inclusion of one ligand-type orbital in the CAS brings Δg_α into good agreement with experiment.[51] For the present Cu fragments, the inclusion of one ligand orbital to the CAS allows a reduction of Δg_α (second set in Table 3) compared to the case of the pure ligand-field CAS (first set in Table 3). However, due to the relatively large ligands in the fragments, this reduction is most probably insufficient, and additional ligand orbitals should be included in the CAS. Such calculations, however, require a large computational effort and have not been undertaken here. We note in relation to this that covalency effects are much less important for lanthanide ions, where reasonable results are expected already for the CAS of ligand-field molecular orbitals only.

Fig. 13 shows the considered model of exchange interactions for complexes **1–4**. Basically, we have 25 exchange coupling constants which, taking into account the symmetry, are grouped in six sets of independent parameters: J_3, J_4, J_5 for Cu···Cu, J_2, J_6 for Cu···Gd and J_1 for Gd···Gd interactions. Due to the structural similarity of **1–4**, the exchange interactions between copper pairs are expected to be similar. Due to the diamagnetism of yttrium, J_1, J_2 and J_6 are zero in the case of Y_2Cu_8. The least-squares fit of the experimental susceptibility for $[Y_2Cu_8]$, performed with the first set of g tensors in Table 3, yielded $J_3 = -44$ cm^{-1}, $J_4 = -40$ cm^{-1} and $J_5 = -24$ cm^{-1}. These parameters were kept fixed in the subsequent simulations of magnetism in Dy_2Cu_8. Fig. 4 shows a comparison between the calculated and measured magnetic susceptibility of $[Y_2Cu_8]$. Due to frustrated antiferromagnetic interactions, the first excited S = 1 exchange term is separated from the ground S = 0 term by only 25 cm^{-1}.

Table 2 Energies (cm^{-1}) of the lowest calculated Kramers doublets for copper fragment models in **1**, in two computational approximations

Nr	Cu1	Cu2	Cu3	Cu4	Cu5	Cu6	Cu7	Cu8
				CASSCF/MS-CASPT2/RASSI CAS (9 in 10)				
1[a]	0.0	0.0	0.0	0.0	0.0	0.0	0.0	0.0
2[a]	9327.9	9587.0	9285.0	8996.4	12446.9	11185.5	12743.4	10813.0
3[a]	9588.1	9765.3	9708.4	9481.4	14467.0	11421.2	14033.3	11235.9
4[a]	11197.9	11372.1	11155.0	10822.2	15530.2	13172.4	15509.5	12995.0
5[a]	12181.8	12371.8	12136.8	11922.3	16793.1	14138.5	16653.5	13937.8
				CASSCF/MS-CASPT2/RASSI CAS (11 in 11)				
1[a]	0.0	0.000	0.000	0.0	0.0	0.0	0.0	0.0
2[a]	9113.1	9793.2	9335.8	9137.7	12412.3	11283.8	12658.2	10963.2
3[a]	9492.8	9890.8	9871.6	9598.2	14531.0	11696.0	14024.8	11547.9
4[a]	11145.6	11377.0	11324.4	10979.8	15645.3	12656.4	15545.0	12458.7
5[a]	12229.6	12809.2	12215.8	11967.2	16881.4	14077.1	16672.3	13932.6
6[b]	13772.3	14595.1	15360.2	12490.2	33167.7	23754.2	36290.9	20875.4
7[b]	25219.1	26101.6	27785.8	26042.2	34502.2	24086.8	40418.2	21109.5
8[b]	29502.4	31981.8	32848.5	30360.5	34907.4	24354.3	40746.7	24151.0
9[b]	33562.8	34173.5	36590.6	34372.4	46857.9	36366.7	53245.0	32736.1
10[b]	34843.9	37692.2	37387.1	35450.5	47391.3	36673.3	53588.4	33059.2

[a] Ligand field states. [b] Ligand–metal charge transfer states.

Table 3 g tensors of individual copper centers in **1** calculated in two computational approximations

Nr	Cu1	Cu2	Cu3	Cu4	Cu5	Cu6	Cu7	Cu8
				CASSCF/MS-CASPT2/RASSI CAS (9 in 10)				
g_x	2.52	2.51	2.49	2.53	2.08	2.09	2.06	2.08
g_y	2.28	2.28	2.31	2.32	2.09	2.10	2.07	2.09
g_z	1.99	2.00	1.99	1.99	2.49	2.49	2.44	2.53
				CASSCF/MS-CASPT2/RASSI CAS (11 in 11)				
g_x	2.46	2.44	2.45	2.48	2.07	2.08	2.07	2.09
g_y	2.30	2.29	2.31	2.31	2.08	2.09	2.08	2.11
g_z	1.99	1.99	1.99	1.99	2.47	2.46	2.43	2.50
				Angle of the main magnetic axes Z with the apical ligand				
	3.08	3.53	4.05	2.76	9.85	9.24	8.85	5.71
				Magnetic susceptibility (χT) at 300 K of a single copper fragment/cm^3 K mol^{-1})				
$\chi T_{300\ K}$	0.505	0.506	0.505	0.511	0.483	0.483	0.474	0.498

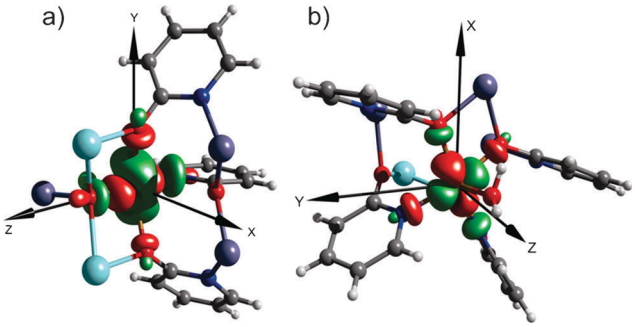

Fig. 12 Singly-occupied molecular orbital in the Cu1 fragment (a) and the Cu5 fragment (b); x, y and z are the main magnetic axes of the ground state g tensors.

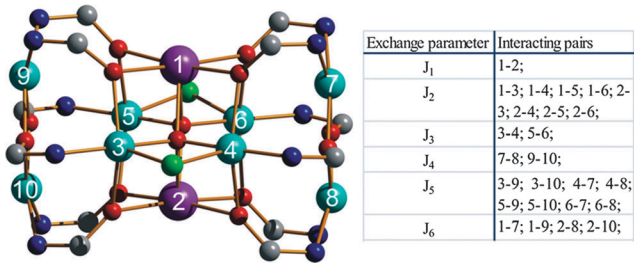

Exchange parameter	Interacting pairs
J_1	1-2;
J_2	1-3; 1-4; 1-5; 1-6; 2-3; 2-4; 2-5; 2-6;
J_3	3-4; 5-6;
J_4	7-8; 9-10;
J_5	3-9; 3-10; 4-7; 4-8; 5-9; 5-10; 6-7; 6-8;
J_6	1-7; 1-9; 2-8; 2-10;

Fig. 13 Model for the exchange interaction considered for complexes **1–4**.

$[Ln_2Cu_8]$ [Ln = Gd(2), Tb(3), Dy(4)]

The calculated fragments containing lanthanide ions are similar to each other. Fig. 14 shows the calculated structure of the model fragment in the case of the Dy ion. The calculated energies of the low-lying spin–orbit states of the lanthanide fragments are listed in Table 4.

For $[Gd_2Cu_8]$ and $[Tb_2Cu_8]$, it was impossible to compute the magnetic properties due to the fact that a very large number of states needed to be considered for the exchange coupling ($2^8 \times 8^2 = 16\,384$ for Gd_2Cu_8 and $2^8 \times 6^2 = 9216$ for Tb_2Cu_8). Nevertheless the single-ion results in Table 2 and Table 3 give some insight into the origin of the SMM behavior. First, the calculated g tensors on Cu sites are strongly anisotropic, even if we expect a further reduction of g_α values in Table 3. This is supported also by the simulations of χT in Y_2Cu_8 (Fig. 4), which required relatively large g_α on copper sites. Cu(II) is an S = 1/2 ion; therefore, its contribution to the anisotropy of the exchange multiplets of the complex can only be *via* anisotropic and antisymmetric exchange interactions. The order of their magnitude is usually estimated as $(\Delta g_\alpha/g)^2$ and $(\Delta g_\alpha/g)$, respectively.[52] The former gives linear and the

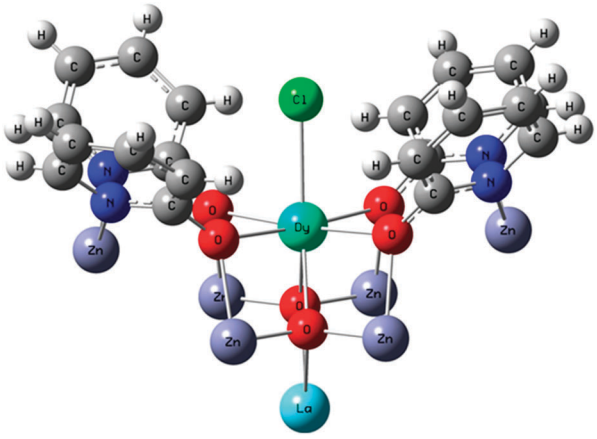

Fig. 14 Structure of the calculated Dy fragment from $[Dy_2Cu_8]$ (**3**).

Table 4 Low-lying energies (cm^{-1}) and g tensors of the spin–orbit states of Ln fragments originating from the corresponding ground atomic multiplet

Gd	Tb	Dy
0.000	0.000	0.000
0.000	6.696	0.000
0.153	12.150	135.445
0.153	42.376	135.445
0.369	47.933	164.542
0.369	86.111	164.542
0.714	143.466	206.752
0.714	181.421	206.752
	212.051	246.550
	292.030	246.550
	306.515	345.024
	383.493	345.024
	385.817	499.767
		499.767
		515.739
		515.739

g tensor for the ground states

	Ground $S = 7/2$	Ground Ising doublet	Ground Kramers doublet
g_x	1.9962	0.0000	0.258
g_y	1.9962	0.0000	0.284
g_z	1.9962	12.3191	19.243

second bilinear contributions to the ZFS of the exchange terms of the polynuclear complex,[53] so they both scale as $(\Delta g_\alpha/g_\alpha)^2$, *i.e.* are strongly dependent on the magnitude of Δg_α. Another contribution is the ZFS on the Ln ion, which amounts to $\approx$0.7 cm^{-1} for Gd in **2** (Table 4). Adding all these contributions will result in a ZFS of the ground exchange term of Gd_2Cu_8 of several cm^{-1}, sufficient to explain the low-temperature blockage of magnetization in this complex (Fig. 6). It is interesting to note that no SMM behavior was found in the related complex Gd_4Cu_5.[46] One of the reason could be the very small Cu–Gd exchange interactions in the latter compound (-0.18 and -0.03 cm^{-1}), [46] for which the states forming the barrier will overlap with the excited exchange states. On the contrary in **2**, the Cu–Gd interaction is expected to be much larger, which can be inferred from the extracted value of Cu–Dy exchange interaction (see below).

In **3**, the Tb–Cu exchange interaction partially restores the magnetic moment on Tb(III), which is quenched by the crystal field splitting of the $J = 6$ ground atomic multiplet of terbium (Table 4). However, compared to **2**, the ionic anisotropy (crystal field splitting) on Tb(III) is the main contribution to the barrier of reversal of magnetization in **3**.

In $[Dy_2Cu_8]$ (**4**), there are $2^8 \times 2^2 = 1024$ exchange states originating from the ground Kramers doublets on the metal sites. Considering the model for the exchange interaction shown in Fig. 13, the best agreement with the experimental data was achieved for the following exchange coupling parameters: $J_1 = +0.25$ cm^{-1}, $J_2 = +2.0$ cm^{-1}, $J_3 = -44$ cm^{-1}, $J_4 = -40$ cm^{-1}, and $J_5 = -25$ cm^{-1}, $J_6 = 0.0$ cm^{-1}. Fig. 9 shows the comparison of the measured and calculated magnetism for Dy_2Cu_8. From the calculation, it is found that the main anisotropy axes on dysprosium ions are oriented along the Dy–Dy bond, as shown in Fig. 15. The surprising result that this compound is the weakest SMM of the present series (it has the smallest coercivity), despite the fact that the entering Dy(III) are magnetic and strongly anistropic (albeit not axial, Table 3), is probably explained by a smaller manifold of states forming the barrier in **4**, as compared to **2**.

Concluding remarks

In this paper, we presented the synthesis, crystal structure and an investigation of the magnetic behavior of a series of $[Ln(III)_2Cu(II)_8]$ decanuclear complexes afforded by 2-hydroxypyridine and Y(**1**), Gd (**2**), Tb(**3**) or Dy (**3**) as the lanthanide ions. All compounds are isomorphs and may be viewed as a hexanuclear central core sandwiched in between two lateral dinuclear copper units. The magnetic properties have been studied *ab initio* by means of fragment calculations. From the calculation of the yttrium complex, it was found that the g tensors of the copper(II) ions are strongly anisotropic, which agree with the experimental data. The yttrium complex, which may be considered as the most simple example, allowed us also to determine the strength and sign of the Cu···Cu magnetic

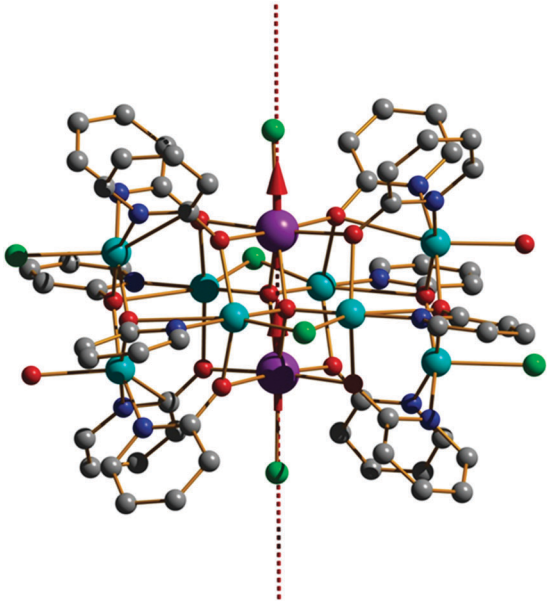

Fig. 15 Orientations of the main anisotropy axes on Dy ions in the ground state of **4**.

interactions. Three sets of antiferromagnetic coupling constants are necessary to fit the experimental data: two within the central ($J_3 = -44$ cm^{-1}) and the lateral ($J_4 = -40$ cm^{-1}) copper dinuclear unit, and one ($J_5 = -24$ cm^{-1}) between the lateral and central copper. The simulation of the magnetic behavior of the Dy (**4**) compound gave $J_1 = +0.25$ cm^{-1} for Dy–Dy and $J_2 = +2.0$ cm^{-1} for Dy–Cu pairs. The anisotropy on the Cu(II) sites, together with the ionic anisotropy of Ln sites, is the reason for the single-molecule magnet (SMM) behavior of **2–4**. A surprising finding is the stronger SMM behavior in **2** compared to **3** and **4**, despite the presence of an isotropic lanthanide (Gd) ion in the former compound. A similar conclusion was recently drawn for the series of M–Ln–M SMMs with M = Co(II) and Fe(III),[54] where the SMM behavior was weakened when moving from Ln = Gd(III) to Ln = Tb(III) and Dy(III). We expect that these counterintuitive results will stimulate further experimental and theoretical investigations of the blockage of magnetization in 4f–3d systems.

Acknowledgements

This work has been supported by the French Minister for Higher Education and Research through a PhD grant to A. B. L. U. acknowledges funding from GOA, INPAC and Methusalem grants from the K. U. Leuven. Single-crystal X-diffraction studies were performed at the "Centre de Diffractometrie Henri Longchambon" at Université Claude Bernard Lyon 1. This work was partially supported by the ANR-PNANO project MolNanoSpin no. ANR-08-NANO-002, ERC Advanced Grant MolNanoSpin no. 226558 and STEP MolSpinQIP.

References

1 G. Christou, D. Gatteschi, D. N. Hendrickson and R. Sessoli, *MRS Bull.*, 2011, **25**(11), 66.
2 D. Gatteschi and R. Sessoli, *Angew. Chem., Int. Ed.*, 2003, **42**, 268–297.
3 (*a*) W. Wernsdorfer, *Adv. Chem. Phys.*, 2001, **118**, 99–189; (*b*) W. Wernsdorfer, N. E. Chakov and G. Christou, *Phys. Rev. B: Condens. Matter Mater. Phys.*, 2004, **70**, 132413.
4 J. Villain, F. Hartman-Boutron, R. Sessoli and A. Rettori, *Europhys. Lett.*, 1994, **27**, 159.
5 R. E. P. Winpenny, *Adv. Inorg. Chem.*, 2001, **52**, 1–111.
6 M. Soler, E. Rumberger, K. Folting, D. N. Hendrickson and G. Christou, *Polyhedron*, 2001, **20**, 1365–1369.
7 E. K. Brechin, C. Boskovic, W. Wernsdorfer, J. Yoo, A. Yamaguchi, E. C. Sanudo, R. Concolino Thomas, L. Rheingold Arnold, H. Ishimoto, N. Hendrickson David and G. Christou, *J. Am. Chem. Soc.*, 2002, **124**, 9710–1.
8 S. K. Ritter, *Chem. Eng. News*, 2004, **82**, 25–30.
9 A. J. Tasiopoulos, A. Vinslava, W. Wernsdorfer, A. Abboud Khalil and G. Christou, *Angew. Chem., Int. Ed.*, 2004, **43**, 2117–21.
10 G. Aromi and E. K. Brechin, *Struct. Bonding*, 2006, **122**, 1–67.
11 O. Kahn, *Molecular Magnetism*, VCH Publishers, New York, 1993.
12 L. F. Chibotaru, L. Ungur, C. Aronica, H. Elmoll, G. Pilet and D. Luneau, *J. Am. Chem. Soc.*, 2008, **130**, 12445–12455.
13 S. Petit, G. Pilet, D. Luneau, L. F. Chibotaru and L. Ungur, *Dalton Trans.*, 2007, 4582–4588.
14 R. Sessoli and A. K. Powell, *Coord. Chem. Rev.*, 2009, **253**, 2328–2341.
15 N. Ishikawa, M. Sugita, T. Ishikawa, S. Koshihara and Y. Kaizu, *J. Am. Chem. Soc.*, 2003, **125**, 8694–8695.
16 N. Ishikawa, M. Sugita and W. Wernsdorfer, *J. Am. Chem. Soc.*, 2005, **127**, 3650–3651.
17 C. Aronica, G. Pilet, G. Chastanet, W. Wernsdorfer, J.-F. Jacquot and D. Luneau, *Angew. Chem., Int. Ed.*, 2006, **45**, 4659–4662.
18 J. P. Costes, F. Dahan and W. Wernsdorfer, *Inorg. Chem.*, 2006, **45**, 5–7.
19 C. Benelli and D. Gatteschi, *Chem. Rev.*, 2002, **102**, 2369–2387.
20 J.-P. Costes, F. Dahan, A. Dupuis and J.-P. Laurent, *Chem.–Eur. J.*, 1998, **4**, 1616–1619.
21 M. L. Kahn, C. Mathoniere and O. Kahn, *Inorg. Chem.*, 1999, **38**, 3692–3697.
22 J. Sanz, L. R. Ruiz, A. Gleizes, F. Lloret, J. Faus, M. Julve, J. Borras-Almenar and Y. Journaux, *Inorg. Chem.*, 1996, **35**, 7384–7393.
23 C. Aronica, G. Chastanet, G. Pilet, B. Le Guennic, V. Robert, W. Wernsdorfer and D. Luneau, *Inorg. Chem.*, 2007, **46**, 6108–6119.
24 S. N. Wang, *Inorg. Chem.*, 1991, **30**, 2252–2253.
25 Nonius, *COLLECT*, Nonius B. V., Delft, The Netherlands, 1997–2001.
26 Z. Otwinowski and W. Minor, *Methods Enzymol.*, 1997, **276**, 307–326.
27 P. W. Betteridge, J. R. Carruthers, R. I. Cooper, K. Prout and D. J. Watkin, *J. Appl. Crystallogr.*, 2003, **36**, 1487.
28 S. Lopez-Moraza, J. L. Pascual and Z. Barandiaran, *J. Chem. Phys.*, 1995, **103**, 2117.
29 A. Sadoc, R. Broer and C. de Graaf, *J. Chem. Phys.*, 2007, **126**, 134709.
30 F. Aquilante, L. De Vico, N. Ferre, G. Ghigo, P.-A. Malmqvist, P. Neograd, T. B. Pedersen, M. Pitonak, M. Reiher, B. O. Roos, L. Serrano-Andres, M. Urban, V. Veryazov and R. Lindh, *J. Comput. Chem.*, 2010, **31**, 224–47.
31 B. A. Hess, C. M. Marian, U. Wahlgren and O. Gropen, *Chem. Phys. Lett.*, 1996, **251**, 365.
32 B. O. Roos, R. Lindh, P.-O. Malmqvist, V. Veryazov and P. O. Widmark, *J. Phys. Chem. A*, 2004, **108**, 2851.
33 P. A. Målmqvist, B. O. Roos and B. Schimmelpfennig, *Chem. Phys. Lett.*, 2002, **357**, 230.
34 L. F. Chibotaru and L. Ungur, *Programs SINGLE_ANISO and POLY_ANISO*, University of Leuven, 2006.
35 M. E. Lines, *J. Chem. Phys.*, 1971, **55**, 2977.
36 D. M. L. Goodgame, D. J. Williams and R. E. P. Winpenny, *Polyhedron*, 1989, **8**, 1913–1921.
37 A. J. Blake, P. E. Y. Milne, P. Thornton and R. E. P. Winpenny, *Angew. Chem., Int. Ed. Engl.*, 1991, **30**, 1139–1141.
38 A. J. Blake, R. O. Gould, P. E. Y. Milne and R. E. P. Winpenny, *J. Chem. Soc., Chem. Commun.*, 1991, 1453–1455.
39 A. J. Blake, R. O. Gould, P. E. Y. Milne and R. E. P. Winpenny, *J. Chem. Soc., Chem. Commun.*, 1992, 522–524.
40 A. J. Blake, P. E. Y. Milne and R. E. P. Winpenny, *J. Chem. Soc., Dalton Trans.*, 1993, 3727–3734.
41 S. N. Wang, Z. Pang and M. J. Wagner, *Inorg. Chem.*, 1992, **31**, 5381–5388.
42 A. W. Addison, T. N. Rao, J. Reedijk and G. C. Verschoor, *J. Chem. Soc., Dalton Trans.*, 1984, 1349–1356.
43 D. J. Watkin, C. K. Prout, J. R. Carruthers and P. W. Betteridge, *CRISTAL Issue 11*, Chemical Crystallography Laboratory, Oxford, UK, 1999.
44 P. van derSluis and A. L. Spek, *Acta Crystallogr., Sect. A: Found. Crystallogr.*, 1990, **46**, 194.
45 C. Benelli, A. J. Blake, P. E. Y. Milne, J. M. Rawson and R. E. P. Winpenny, *Chem.–Eur. J.*, 1995, **1**, 614–618.
46 S. K. Langley, L. Ungur, N. F. Chilton, B. Moubaraki, L. F. Chibotaru and K. S. Murray, *Chem.–Eur. J.*, 2011, in press.
47 L. F. Chibotaru, L. Ungur and A. Soncini, *Angew. Chem., Int. Ed.*, 2008, **47**, 4126–4129.
48 L. Ungur, W. Van den Heuvel and L. F. Chibotaru, *New J. Chem.*, 2009, **33**, 1224–1230.
49 L. F. Chibotaru, M. F. A. Hendrickx, S. Clima, J. Larionova and A. Ceulemans, *J. Phys. Chem. A*, 2005, **109**, 7251–7257.
50 H. Bolvin, *ChemPhysChem*, 2006, **7**, 1575–1589.
51 S. Vancoillie and K. Pierloot, *J. Phys. Chem. A*, 2008, **112**, 4011–4019.
52 T. Moryia, in *Magnetism*, ed. G. T. Rado and H. Suhl, Academic Press, New York, 1963, pp. 85.
53 A. Bencini and D. Gatteschi, *EPR of Exchange Coupled Systems*, Springer Verlag, Berlin, 1990.
54 T. Yamaguchi, J. P. Costes, Y. Kishima, M. Kojima, Y. Sunatsuki, N. Brefuel, J. P. Tuchagues, L. Vendier and W. Wernsdorfer, *Inorg. Chem.*, 2010, **49**, 9125–9135.